BNL-68340

IN SITU STUDIES OF CORROSION USING X-RAY ABSORPTION NEAR SPECTROSCOPY (XANES)

by
H.S. Isaacs , P. Schmuki, and S. Virtanen

for the proceedings volume

199th Meeting - Washington, D.C.
March 25-30, 2001
STATE OF THE ART APPLICATION OF SURFACE AND INTERFACE ANALYSIS METHODS TO ENVIRONMENTAL MATERIAL INTERACTIONS
Edited by
D.R. Baer, **C.R. Clayton**, **G.P. Halada**, and **G.D. Davis**

IN SITU STUDIES OF CORROSION USING X-RAY ABSORPTION NEAR SPECTROSCOPY (XANES)

H.S. Isaacs[1], P. Schmuki[2], and S. Virtanen[3],

[1] Materials Science Division, Energy Sciences and Technology Department, Brookhaven National Laboratory, Upton, NY 11973, USA

[2] Chair for Surface Science and Corrosion (LKO), Department for Material Science Friedrich-Alexander University Erlangen-Nuremberg, D-91058 Erlangen, Germany

[3] Institute for Materials Chemistry and Corrosion, Swiss Federal Institute of Technology, ETH-Hönggerberg, CH-8093 Zürich, Switzerland

ABSTRACT

Applications of x-ray absorption near-edge spectroscopy (XANES) and the design of cells for in situ corrosion studies are reviewed. Passive films studies require very thin metal or alloy layers be used having a thickness of the order of the films formed because of penetration of the x-ray beam into the metal substrate. The depth of penetration in water also limits the thickness of solutions that can be used because of water reduces the x-ray intensity. Solution thickness must also be limited in studies of conversion layer formation studies because the masking of the Cr in solution. Illustrative examples are taken from the anodic behavior of Al-Cr alloys, the growth of passive films on Fe and stainless steels, and the formation of chromate conversion layers on Al.

INTRODUCTION

The purpose of this presentation is to describe a number of applications of x-ray absorption near edge spectroscopy (XANES) that have been used to study corrosion related processes. The employment of x-ray absorption techniques makes it possible to observe chemical changes during electrochemical measurements that cannot be made in situ, using other available techniques. Realtime response enables a direct, unambiguous correlation with controllable variables. In the area of corrosion XANES has a particular advantage because of its sensitivity. It is possible to specify the chemistry changes of less than a monolayer of an element as it undergoes electrochemical reactions of dissolution.

The acquisition of EXAFS data is essentially the same as that of XANES but generally requires a larger amount of the element being studied. EXAFS has the advantage of yielding structural data relating to nearest neighbors where no long range order exists. In situ electrochemical x-ray scattering techniques with noble metals have also been used to detect two-dimensional structural changes in surface layer of the metal following potential changes or following an underpotential metal deposit or an oxidation

process. The structure of a three-dimensional passive oxide of the order of a few monolayers on iron has also been defined using in situ electrochemical techniques. Details of these methods have appeared in recent publications (1-3).

X-ray absorption spectra are obtained with a monochromatic x-ray source (4). When the x-ray photon energy increases above a threshold, or observed edge, for the excitation of an inner core electron the absorption increases and the kinetic energy of the excited electron increases with photon energy above the threshold. XANES occupies up to about 40 eV above the edge and the EXAFS occurs above this energy. Figure 1 contrasts the major differences between XANES and EXAFS (4). In EXAFS the photoelectron is scattered only by a single neighbor, whereas in XANES there are multiple scattering pathways. Analysis of structural relation in XANES is far more complex than for EXAFS, but recent calculations demonstrate that XANES spectra can also be used to determine bond distances of neighboring atoms (4).

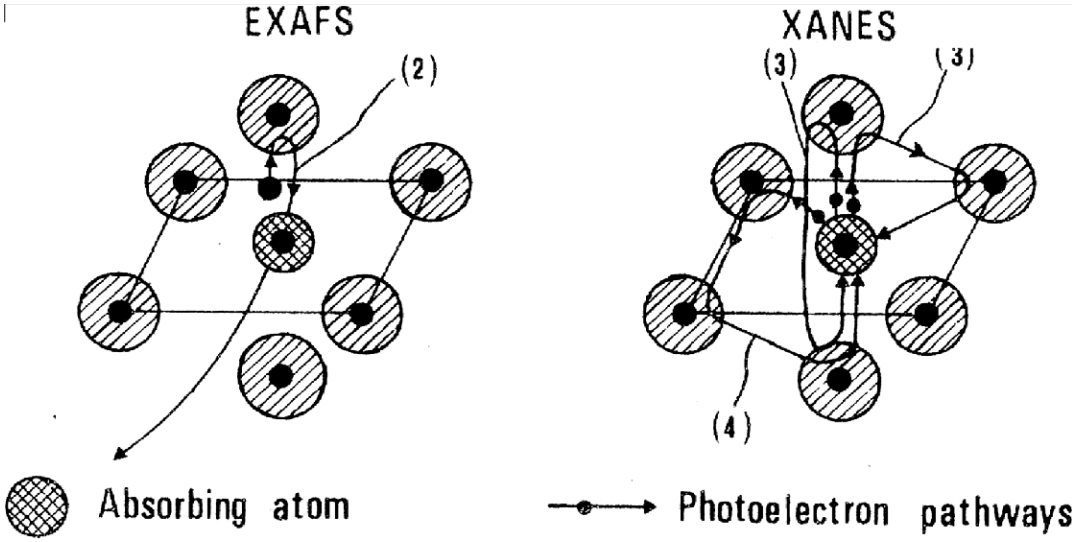

Figure 1. Pictorial view of photoelectron scattering processes. EXAFS results from a single scattering of the photoelectron by a neighboring atom. In XANES multiple scattering pathways, illustrated by 2 to 4, contribute to the absorption cross section. (After Bianconi Ref (4)).

Most corrosion applications rely on spectra of known standards that are used as "thumbprints" for identification of the reactants and products. An example of the edges for a series of Fe and Cr compounds are shown in Figure 2. To compare compounds they are generally normalized relative to the effective step height of the edge. Design of the experimental electrochemical cell is of major importance in making in situ x-ray absorption measurements and must take into account the path of the beam. Illustrative examples of cell designs for studies of passive films on metals and the behavior of a surface inhibitor will be considered. Figure 3 shows the penetration depth of an x-ray beam in water polyester and Fe. Included in the figure are the energies of the K-edges for the elements S to Ag (3). The penetration in Fe is also given over this energy range showing the edge that occurs at 7112 eV. The penetration depth at this energy is of the order of 10 μm (decreasing from about 40 to 4 μm as the energy crosses the absorption

edge) for iron but decreases when studying lighter elements. The passive oxide on metal is of the order of 4 nm thick. Hence, if a measurement was made directly on bulk Fe the oxidized Fe absorption in the passive oxide will be swamped by the metal absorption by

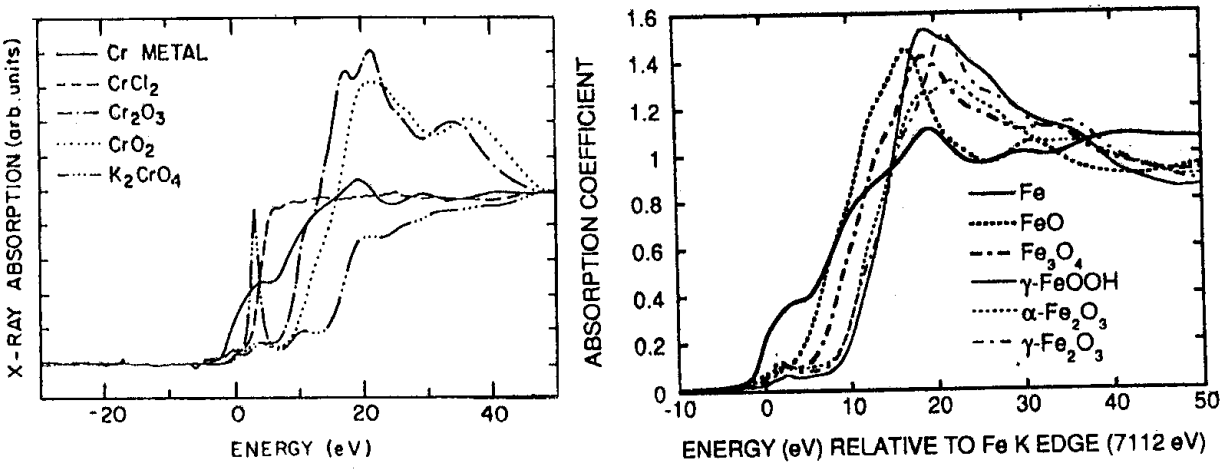

(a) **(b)**

Figure 2. XANES for (a) Cr and Cr compounds, relative to the Cr K edge at 5989 eV (5) and (b) Fe and Fe compounds (6).

about four orders of magnitude. This necessitates that the thickness of the metal be reduced to that comparable with the thickness of the oxide in order to observe changes in the passive film as it is formed, dissolved or reduced. Figure 3 also shows the penetration depth for water. In the range of the absorption energy of Fe the mean free path or penetration depth in water is about 3 mm. This thickness is reduced with dissolved salts in the water.

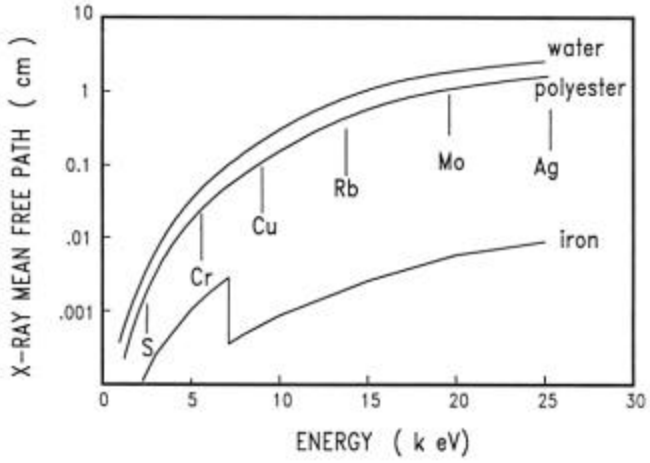

Figure 3. Changes in the x-ray mean free path, or distances for a 1/e reduction of x-ray intensity in water, polyester and Fe, as a function of the x-ray energy. The energies of the K absorption edges for a series of elements are indicated (3,7).

Thin layer metal electrodes about 10 nm thick are required in order to study the passivation of metals and alloys (8-10). An example of a cell employing thin evaporated or sputtered layers of metal is shown in Figure 4a (10). The metal to be monitored is deposited on a thin 7 μm plastic sheet with an underlying inert metal that acts as a current collector. The metal, under potential control, is the working electrode in an electrochemical cell. The x-ray beam then enters through the plastic and the metal. The fluorescence of the metal is proportional to the absorption and is monitored with a solid

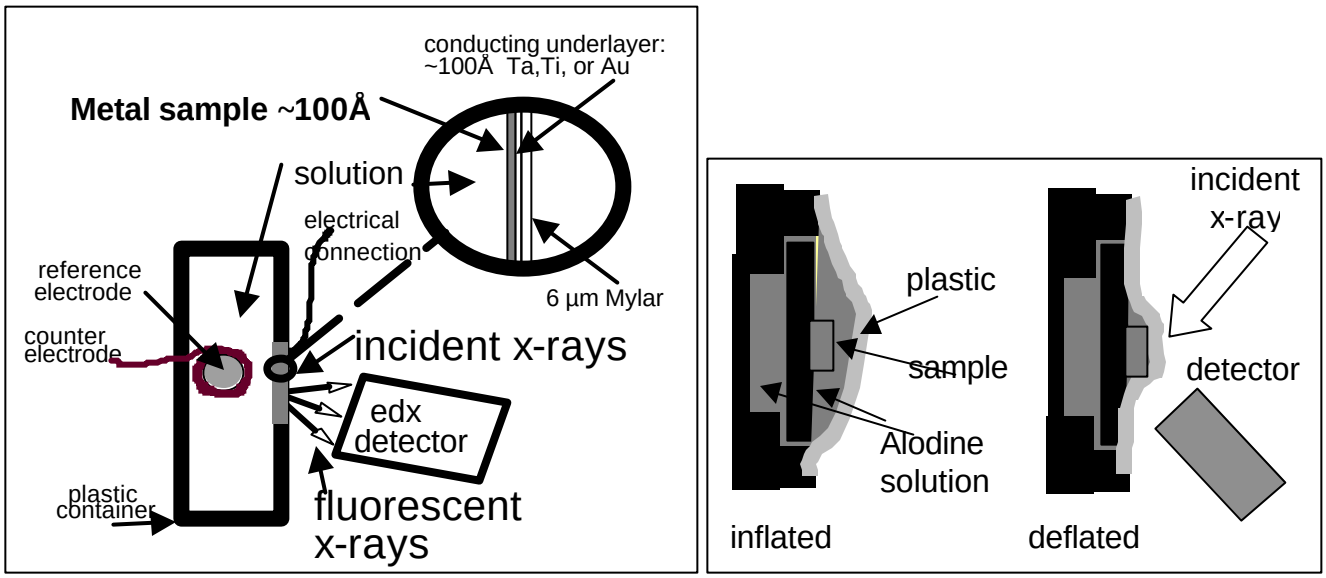

(a) **(b)**

Figure 4. Schematic diagrams of cells used for corrosion studies. (a) Cell for observing formation and dissolution of passive surfaces (10). (b) Cell for observing growth of chromate conversion coatings (11).

state detector to reduce the background due to scattered radiation. Entering the back of the metal prevented difficulties with the aqueous electrolyte absorbing the x-ray beam.

The in situ measurements are complicated by the penetration of the electrolyte by the beam and care is required to reduce the contribution of the dissolved inhibitor. A concentration of 10^{-5} molar inhibitor in 1 mm of solution above a surface would be equivalent to about a adsorbed monolayer of the inhibitor indicating that concentrations below 10^{-4} molar could be used for this geometry and a fluorescence measurement. Other approaches have been used similar to those where studies of structures on metal surfaces have been carried out (12-13). Here, under a negative hydrostatic pressure, a thin plastic membrane is pressed against the metal surface after the electrochemistry has been completed so the diffraction measurements can be carried out without interference by the electrolyte. Figure 4 b shows an adaptation of this approach used for studying the formation of a chromate conversion layer on Al (11).

Studies of inorganic layers on metal surfaces have been carried out ex situ using glancing angle techniques (5, 12-18). When flat surfaces are used advantage is taken of the refractive index of solids being slightly less than unity, and at a sufficiently low glancing angles the x-ray beam is totally reflected. The intensity of the x-ray beam at the surface is increased under these conditions and is a maximum at the critical angle for total reflection. The penetration depth of the wave also increases from about 2 nm well below the critical angle and rapidly above 10 nm as the critical angle is exceeded.

EXAMPLES OF THE APPLICATION OF XANES

Passive Films on Al-Cr sputtered alloys.

Amorphous Al-Cr alloys have been shown to possess a high resistance to pitting corrosion in chloride solutions. The distribution of Cr and its valence state has been considered to be important in understanding the resistance to pitting (5, 10, 19).

Using ex situ glancing angle techniques Frankel et al have shown that the Cr in the passive oxide film was present either in the chromic, Cr(III) state or as a hexavalent Cr(VI) species depending on the potential pretreatment of the Al-Cr alloy (5). Alloys with concentrations up to 46% Cr were tested. Figure 5 shows the XANES for a 4 nm thick Al 20% Cr alloy following holding at –0.5 to 5.0 V relative to a mercurous sulfate electrode in a pH 7.4 borate buffer solution for 5 min. It is of interest to note that these measurements with a good signal to background noise have an equivalent thickness of Cr of roughly 0.8 nm or two monolayers of Cr. Distinct changes in the chemistry of the Cr can be assessed by comparing with the standards shown in Figure 2. At -0.5 Vmse 82% of the Cr remained as metallic Cr(0) and 18% was present as Cr(III). At 0.7 V, a potential well above that where highly soluble Cr(VI) is thermodynamically expected (–0.08 $_{Vmse}$ (20)), about 45% of the Cr was oxidized and present only as Cr(11I). Cr(VI) was observed at 2.0 and 5 V_{mse} increasing dominant as the oxidized species. The degree of oxidation depended on the measurement angle being greater below the critical angle than just above it, demonstrating higher concentration of Cr(VI) closer to the outer

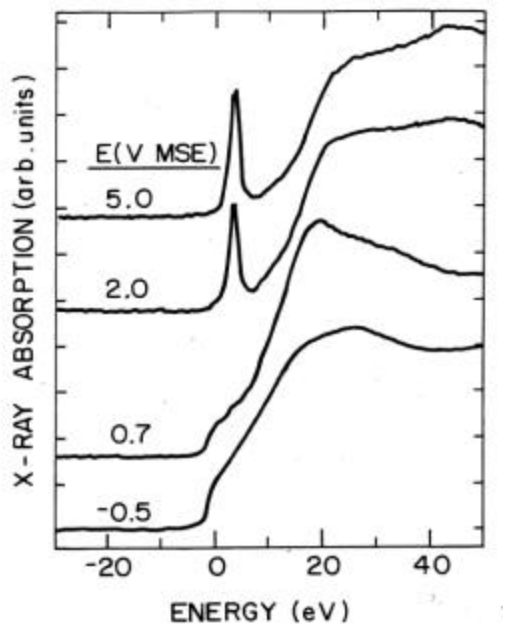

Figure 5. Influence of applied potential in a borate solution on the Cr K absorption edge, for a 20% Cr-Al sputtered 40Å film measured ex situ (5).

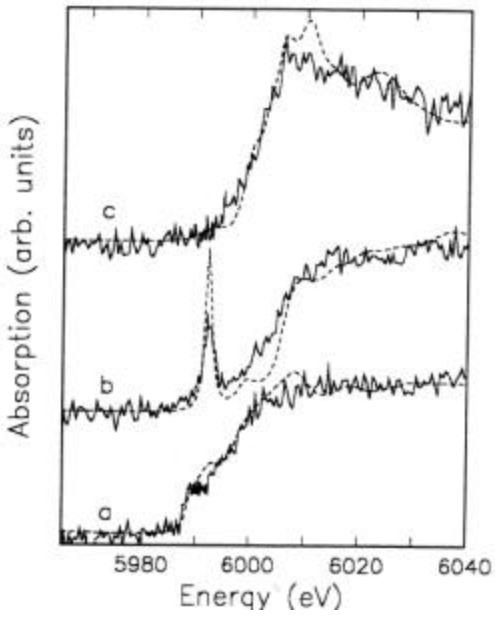

Figure 6. In situ measurements of the Cr K edge for a 20 Å, 12%Cr-Al film (solid lines) (a) at open circuit, (b) after 7 min at $2V_{mse}$, (c) after 6 min at –1.5 V_{mse}. Broken lines are standards for (a) Cr metal, (b) K_sCrO_4, and (c) Cr_2O_3 (10).

surface of the oxide.

When in situ measurements were made (19), using the cell shown in Figure 4a, the in situ results again showed virtually no dissolution when the potential was raised directly to 1.5 or 2 V_{mse}. The in situ measurements did allow for a clearer analysis of the process taking place during the exposure to the high potential. It was also found that the Cr(VI), formed at the higher potentials, could be converted to Cr(III) on stepping the potential to –1.5 V_{mse} (10). Cycling the potential repeated the valence changes with very little loss of the Cr even in the highly soluble Cr(VI) state. An example of the electrochemical response of the Cr in the oxide is shown in Figure 6.

Figure 7 shows the effect of time on stepping a freshly exposed Cr-Al film directly to 2 $_{Vmse}$ (19). The sample had a lower 12% Cr content that produced a slower rate of Cr(VI) formation in the oxide. Here in the first 6 minutes the first stages of oxidation at 2 V_{mse} are seen to be the Cr(III) formation. This was then followed by a slow oxidation to Cr(VI). Two distinct stages may be envisaged in the rapid oxidation. Following the potential step the high field across the initially thin air formed oxide film produced a very rapid growth dominated by the activity of Al which suppressed the oxidation of the Cr so only Cr(III) species are formed. The rate of high field oxidation decreases exponentially with time, and then by a slower process the oxidation of Cr(III) to Cr(VI) oxidation took place. The oxidation of the Cr in the oxide to Cr(VI) is unlikely

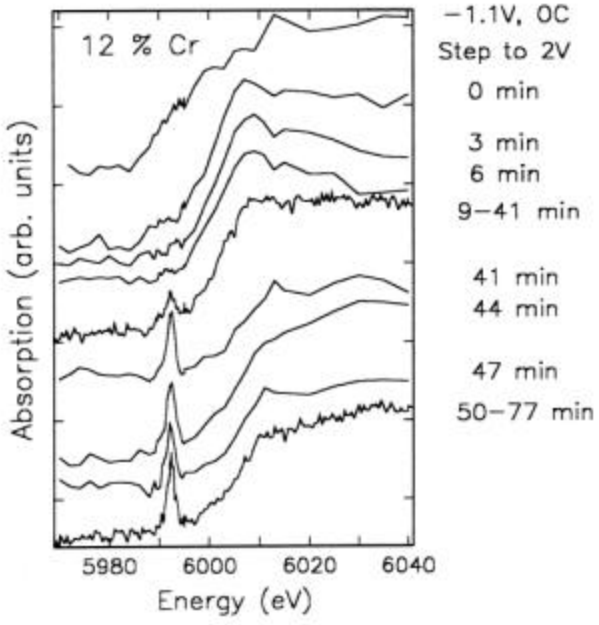

Figure 7. Changes in the Cr K edge at the times indicated at 2 V_{mse} in a borate solution, after stepping from the open circuit potential

to result from oxygen migration in the oxide as this takes place only under high fields which rapidly decrease after the potential is stepped. Hydroxyl ions could be involved. Hydroxyl ions have been considered to migrate during the oxide growth (21) or else a slow hydrolysis of the oxide may take place after its formation probably assisted by the presence of the Cr because the 20%Cr content in Figure 6 led to a faster oxidation rate (< 5 min) than the 12% Cr in Figure 7, which took between 20 and 40 min. The oxidation according to the equation

$$Cr^{3+} + 4OH^- = CrO_4^{2-} + 4H^+ + 3e^-$$

would require only the movement of electrons and hydrogen in the oxide which are expected to be far more mobile than oxygen ions.

The in situ study made it convenient to step the potential in small increments. This treatment resulted in very different behavior from that observed on direct stepping to the higher potentials (18). Indeed, dissolution of an entire fresh Al-Cr alloy sample took place when it was exposed directly to a potential of 0.2 V_{mse} or when the potential was slowly raised to this value. It was hypothesized that a layer of aluminum oxide formed initially when the potential was stepped to the high potential and prevented the Cr(VI) from entering the solution. Studies by Kihn et al using electron energy loss spectroscopy have since confirmed that the Al does preferentially oxidize during rapid anodic film growth allowing buildup of Cr in the metal (22). When the potential is slowly increased, no outer continuous Al oxide forms, and in its absence any Cr(VI) has in continued access to the solution and percolation of the entire sample occurs.

Passive Films on Iron

Early XANES studies on passivity of Fe have been reviewed by Robinson (23). These and subsequent detailed studies of the passivity of Fe and its alloys have shown that XANES continues to yield information, difficult to obtain using other techniques, relating to changes that take place in the passive film during its formation and reduction (24-32).

XANES has clarified the changes taking place during passive film reduction on Fe. Davenport et al showed that the ferric oxide passive film in borate buffer dissolved during controlled galvanostatic cathodic reduction to produce ferrous ions in solution (24). During the reduction process the remaining film showed a change towards Fe_3O_4. In alkaline solution reduction of the passive film produced a ferrous oxide or hydroxide without any dissolution taking place (24). These changes were reproduced by Schmuki et al using thin layers of ferric oxide and magnetite as artificial passive films (25,26). A comprehensive model was proposed for the reduction process in aqueous solutions. Reduction starts at oxide solution interface with a solid state reaction transforming the Fe_2O_3 to Fe_3O_4 and producing a two layer structure. In a second reduction step the Fe_3O_4 is reduced to Fe^{2+} which dissolves (25). The second step was slow in neutral solution until the entire Fe_2O_3 phase was converted to Fe_3O_4 at which stage any further reduction led to the Fe_3O_4 dissolution. In sulfuric acid solutions the Fe_3O_4 phase dissolves so that the first stage is rate determining in the removal of the passive film. In alkaline solutions, a solid state reduction of the Fe_3O_4 phase takes place with the formation of $Fe(OH)_2$ (25). Stepping the potential produces similar end products except in the presence of phosphate ions as described by Schmuki et al in these proceedings (26). When phosphate is present potentiostatic stepping to negative potentials produces a metallic Fe without any dissolution.

The passive film forms with 100% efficiency, i.e. no Fe dissolution, when the potential of an oxide free surface is stepped well into the passive region in a 0.136 M borate pH 8.4 solution (42-30). The efficiency of passive film formation has been studied by Oblonsky et al (27, 28) and Virtanen et al (30) as a function of potential and solution chemistry. For example in 0.136 M borate buffer, pH 8.4, or 0.1M PO_4 also having a pH

8.4 stepping to potentials below -0.7 V_{mse} or 0.8 V_{mse}, respectively, produced dissolution that increased as the potential decreased (27). Dissolution was also observed when the borate was diluted to 0.01M (pH 8.4), or the pH was reduced to 7.4 (0.138 M BO_3) (28). These latter results are shown in Figure 8. The figure compares the XANES of the Fe sample before and after stepping into the passive range. Prior to stepping the edge indicates that the Fe was only in the metallic state. Immediately after stepping to 0.4 V_{mse} the height of the edge dropped showing that dissolution of metal took place during passivation. A greater drop was found following stepping the potential in a solution with the decreasing the pH to 7.4 compared with diluting the borate buffer but maintaining the pH at 8.4. In acetate solutions, detectable dissolution rates occurred above pH 5 whereas significant dissolution occurred below this value (27). Again lower electrolyte concentrations produced more dissolution. The investigation showed dissolution was transitory in all cases, occurring only during the initial stages of passivation. XANES measurements were too slow and could not resolve times less than about 2 min. The measurements in acetate solutions also emphasized the role of reductive dissolution where the complementary anodic process for oxide reduction was metal dissolution and not only the measured external current (28).

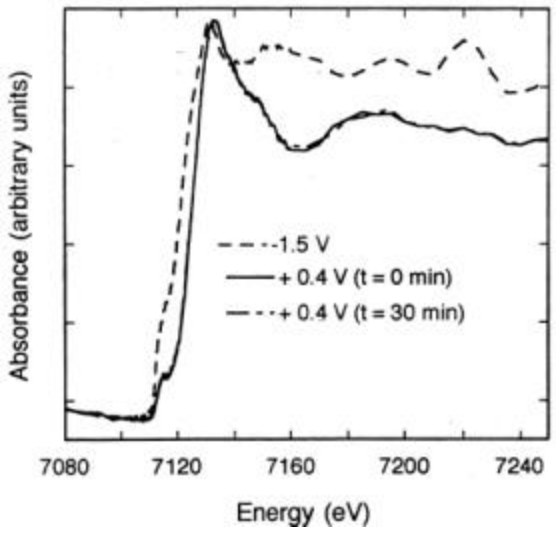

Figure 8. Changes in the edge spectra for Fe on stepping the potential from –1.5 V_{mse} to 0.4 V_{mse} in a pH 8.4, 0.01 M borate solution taken immediately after stepping and after 30 min. Dissolution of metal took place in the dilute borate solution only during film formation (27).

Passive Films on Fe-Cr Stainless Steels

The composition of passive films on stainless steels depends on the pretreatment history of the steel and has been reviewed in detail by Oblonsky et al (29). Fe can be prepared with metallic surfaces by cathodic dissolution of the passive surface. When Cr is present, the Cr(III) in the oxide cannot be cathodically reduced. In acetate solutions it was found that all the Fe in the oxide was removed at –1.2 V_{mse} (29). Stepping from this potential to –0.3 V_{mse}, just above the passivation peak, produced a high Cr content in the oxide which varied from 60 to 100% Cr(III) as the alloy concentration increased from 8 to 23% Cr. Stepping directly to 0.2 V_{mse} the passive film content dropped varying form 20 to 60% over the same alloy concentration (29). Within the region of transpassivity the passive film contains Cr(VI) (27,28). In the acetate solutions a fraction of 0.25 was found as Cr(VI). It was found that the Cr(VI) was unstable when exposed in humid air, leading to Cr(VI) reduction (30). The XANES measurements offered direct evidence for the reduction of Cr(VI) that was postulated based on transients during galvanostatic reduction. It is interesting to note that there was no indication of Cr(VI) reduction when the Al-Cr samples were exposed to air (5) even though the thermodynamic driving

potential for Al is much greater than for Fe. Also the reduction indicated that the exposure to oxygen in air did not lead to oxidation. Clearly for these oxides reactions, kinetics, rather than thermodynamic potential magnitudes, are decisive.

Schmuki et al have also used XANES to study the chemical states and dissolution rates of artificial passive films containing Fe and Cr (32). In intermediate ranges of Cr concentrations the oxides were resistant to dissolution in borate buffer solutions at both anodic and cathodic potentials. Nevertheless, in all cases, even when no dissolution takes place the oxides were electrochemically active. Reduction of Fe(III) to Fe(II) and oxidation of Cr(III) to Cr(VI) were observed. The Fe(III) reduction penetrated the entire oxide but the Cr(VI) formation occurred only to a depths of a few atomic layers. In 0.1 M H_2SO_4 50% Cr was required to prevent cathodic dissolution and 90% Fe was necessary to prevent the dissolution of Cr (32).

Chromate conversion coatings (CCC).

Chromate/fluoride solutions (e.g. commercial product Alodine 1200) produces a Cr(III)/Cr(VI) coating that has been used extensively to prepare Al and its alloys for corrosion protection and paint adhesion (11,17,33-39). Studies of the CCC on Al alloy 2024 have been made ex situ using a wide range of techniques (32-39). X-ray absorption measurements have shown the amounts Cr(VI) to total Cr in the CCC vary from 15% for pure Al to between 20 and 28% for AA 2024 (11,17,33,36). Coating times led to increases of Cr(VI) from 11 to 20% for exposures of 1 to 5 min (17). The formation of the CCC is rapid and cooling the chromate/fluoride solution has been used to slow the rates (38,39) or by restricting the accesses of solution as shown by the cell in Figure 4 b.

Figure 9 shows the increase in the edge height as a function of the time of repeated exposures of alloy AA2024 to the Alodine solution up to 600 s. The rate of formation of the CCC was a complex function of time. During the very first exposure and for about 10 s the uptake of Cr was extremely rapid producing about 10% of the film thickness. The changes were indicative of an exponentially decreasing rate with a time constant of the order of seconds. The rate then varied more slowly reaching a second maximum after 140 s. Prior to 140 s the Cr(VI) increased slowly to from about 28 to 35% and remained constant thereafter as the coating continued to thicken. The very rapid initial reaction rate caused the difficulty in producing very thin CCC layers and the required cooling of the solution (38,39) in order to measure the early stages of nucleation and growth of the coating.

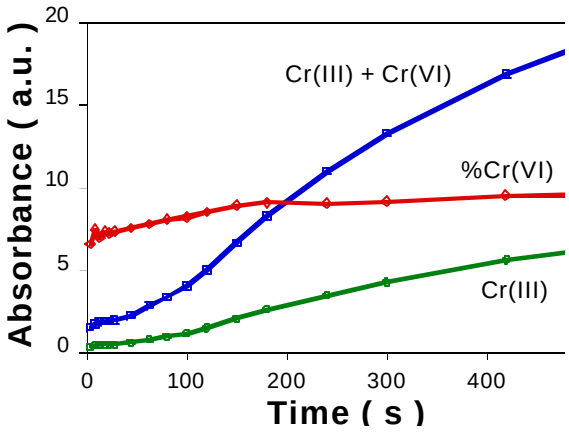

Figure 9. In situ changes of Cr species during growth of a chromate conversion coating on an Al alloy 2024 on exposure to Alodine 1200 (11).

ACKNOWLEDGMENTS

This work was carried out, in part, under the auspices of the U.S. Department of Energy, Division of Materials Sciences, Office of Basic Energy Sciences under Contract No. DE-AC02-98CH10886. The XANES experiments were performed at the National Synchrotron Light Source, beamlines X10C and X18B.

REFERENCES

1. C. A. Melendres and A. Tadjeddine, Editors, *Synchrotron Techniques in Interfacial Electrochemistry*. Kluwer Academic Press, Dordrecht, (1994).
2. A. Davenport and J. G. Gordon II, Editors, *X-ray Methods in Corrosion and Interfacial Chemistry*. PV **92-1**, The Electrochemical Society Proceedings Series, Pennington, NJ (1992).
3. F. W. Lytle, in *In Situ Characterization of Electrochemical Processes,* National Academy Press, Washington DC, (1987).
4. A. Bianconi, in *X-ray Absorption*, D. C. Koningsberger and R. Prins, Editors, p. 573, John Wiley & Sons, New York, (1998).
5. G. S. Frankel, A. J. Davenport, H. S. Isaacs, A. G. Schrott, C. V. Jahnes, and M. A. Russak, J. Electrochem. Soc. **139**, 1812 (1992).
6. A. J. Davenport, private communication.
7. H. S. Isaacs, in Ref.1, p.199.
8. G. G. Long, J. Kruger, D. R. Black and M. Kuriyama, J. Electroanal. Chem., **150**, 603 (1983).
9. M. Kerkar, J. Robinson and A. J. Forty, Faraday Discuss. Chem. Soc., **89**,31 (1990).
10. A. J. Davenport, H. S. Isaacs, G. S. Frankel, A. G. Schrott, C. V. Janes and M. A. Russak, J. Electrochem Soc., **138**, 337 (1991).
11. C. Jeffcoate and H. S. Isaacs, to be published.
12. M. G. Samant, M. F. Tony, G. L. Borges, L. Blum and O.R. Melroy, Surf. Sci., **193**, L29 (1988).
13. A. J. Davenport, L. J. Oblonsky, M. P. Ryan, M. F. Toney. J. Electrochem. Soc., **147**, 2162. (2000).
14. L. G. Parratt, Phys. Rev. **95**, 359 (1956).
15. A. J. Davenport and H. S. Isaacs. Corros. Sci. **31**, 105 (1990).
16. A. J. Davenport, H. S. Isaacs, and M. W. Kendig, J. Electrochem. Soc. **136**, 1837 (1989).
17. M. W. Kendig, A. J. Davenport, and H. S. Isaacs, Corrosion Sci., **34**, 41 (1993)
18. P. Borthen, H. H. Strehblow, Journal de physique, IV, **7**, 695 (1997).
19. G. S. Frankel, A. G. Schrott, A. J. Davenport, H. S. Isaacs, C. V. Jahnes, and M. A. Russak, J. Electrochem. Soc. **141**, 83 (1994).
20. M. Pourbaix, *Atlas of Electrochemical Equilibria in Aqueous Solutions*, NACE Houston and CEBELCOR, Bruxelles (1974).
21. T. P. Hoar and N. F. Mott, J. phys. Chem. Solids, **9**, 97 (1959).
22. Y. Kihn, G.E. Thompson, G. Galaup, P. Skeldon , X. Zhou, K. Shimizu, H. Habazaki, Corrosion Sci., **42** 533 (2000)
23. J. Robinson, in Reference 2, p. 239.
24. A. J. Davenport, J. A. Bardwell and C. A. Vitus, J. Electrochem. Soc. **142**, 721 (1995).

25. P. Schmuki, S. Virtanen , A. J. Davenport and C. A. Vitus, J. Electrochem. Soc. **143**, 574 (1996).
26. P. Schmuki, S. Virtanen, H. S. Isaacs, These Proceedings.
27. L. J. Oblonski, A. J. Davenport, M. P. Ryan, H. S Isaacs and R. C. Newman, J. Electrochem. Soc. **145**, 1922 (1998.
28. L. J. Oblonski, M. P.Ryan and H. S Isaacs, Corros. Sci. **42**, 229 (1990).
29. L. J. Oblonski, M. P.Ryan and H. S Isaacs, J. Electrochem. Soc. **145**, 1922 (1998).
30. S. Virtanen, P. Schmuki, M. Buchler and H. S. Isaacs, J. Electrochem. Soc. **146**, 4087 (1999).
31. J. A. Bardwell, G. I. Sproule, D. F. Mitchell, B. MacDougall and M.J. Graham, J. Chem. Soc. Faraday Trans., **87**, 1011 (1991).
32. P. Schmuki, S. Virtanen, H. S. Isaacs, M. P. Ryan, A. J. Davenport, H. Bohni, and T. Stenberg, **31**, 105 (1990).
33. F.W. Lytle, R.B. Greegor, G.L. Bibbins, K.Y. Blohowiak, R.E. Smith and G.D. Tuss, Corros. Sci., **37**, 349 (1995).
34. P.L. Hagans and C.M. Haas, ASM Handbook, Vol. 5, p. 405, ASM international, Metals Park, OH (1994).
35. L. Xia and R.L. Mc Creery, J. Electrochem. Soc., **145**, 3083 (1998).
36. C. S. Jeffcoate, H. S. Isaacs, A. J. Aldykiewicz, and M. P. Ryan, J. Electrochem. Soc., **147**, 540 (2000).
37. V. Laget, C. Jeffcoate, H.S. Isaacs, R.G. Buchheit, Unpublished
38. G. M. Brown, K. Shimizu, K. Kobayashi and G. E. Thompson, **33**, 1371 (1992).
39. J. R. Waldrop and M. W. Kendig, J. Electrochem. Soc. **145**, L11 (1998).